REFERENCES
1. W. Kern and D. A. Puotinen, *RCA Rev.*, **31,** 187 (1970).
2. A. Ishizaka and Y. Shiraki, *This Journal*, **133,** 666 (1986).
3. G. Gould and E. A. Irene, *ibid.*, **134,** 1031 (1987).
4. E. Yablonovich, D. L. Allara, C. C. Chang, T. Gmitter, and T. B. Bright, *Phys. Rev. Lett.*, **57,** 249 (1986).
5. M. Miyawaki and T. Ohmi, *IEEE Electron Device Lett.*, **EDL-11,** 448 (1990).
6. M. Morita, T. Ohmi, E. Hasegawa, M. Kawakami, and M. Ohwada, *J. Appl. Phys.*, **68,** 1272 (1990).
7. T. Sunada, T. Yasaka, M. Takakura, T. Sugiyama, S. Miyazaki, and M. Hirose, in Extended Abstracts of the 22nd Conference on Solid State Devices and Materials, Sendai, Japan, S-F-3, p. 1071 (1990).
8. M. Morita, T. Ohmi, E. Hasegawa, M. Kawakami, and K. Suma, *Appl. Phys. Lett.*, **55,** 562 (1989).
9. K. Sugiyama, T. Igarashi, K. Moriki, Y. Nagasawa, T. Aoyama, R. Sugino, T. Ito, and T. Hattori, *Jpn. J. Appl. Phys.*, **29,** L2401 (1990).
10. Y. Kobayashi and K. Sugii, *ibid.*, **29,** 1004 (1990).
11. T. Aoyama, T. Yamazaki, and T. Ito, *Appl. Phys. Lett.*, **61,** 102 (1992).
12. T. Aoyama, T. Yamazaki, and T. Ito, *This Journal*, **140,** 366 (1993).
13. J. R. Vig, *J. Vac. Sci. Technol.*, **A3,** 1027 (1985).
14. H. Okabe, *Photochemistry of Small Molecules*, p. 184, John Wiley & Sons, Inc., New York (1978).
15. L. D. Bell, W. J. Kaiser, M. H. Hecht, and F. J. Grunthaner, *Appl. Phys. Lett.*, **52,** 278 (1988).
16. M. Grundner and H. Jacob, *Appl. Phys.*, **A39,** 73 (1986).
17. Y. J. Chabal, G. S. Higashi, K. Raghavachari, and V. A. Burrows, *J. Vac. Sci. Technol.*, **A7,** 2104 (1989).
18. S. Watanabe, M. Shigeno, N. Nakayama, and T. Ito, *Jpn. J. Appl. Phys.*, **30,** 3575 (1991).
19. R. Sugino, Y. Nara, H. Horie, and T. Ito, *J. Appl. Phys.*, **76,** 5498 (1991).
20. T. Aoyama, T. Yamazaki, and T. Ito, *This Journal*, **140,** 1704 (1993).
21. Y. Kobayashi and K. Sugii, *J. Vac. Sci. Technol.*, **B9,** 748 (1991).

Hydrogen Electrocatalysis by Carbon Supported Pt and Pt Alloys

An *In Situ* X-Ray Absorption Study

Sanjeev Mukerjee* and James McBreen*

Brookhaven National Laboratory, Department of Applied Science, Material Science Division, Upton, New York 11973, USA

ABSTRACT

In situ x-ray absorption spectroscopy (XAS) in 1 *M* $HClO_4$ was used to examine the electronic and structural effects of hydrogen adsorption on carbon supported Pt (Pt/C) and Pt alloyed with first row transition metals (Cr, Mn, Fe, Co, and Ni). In the case of Pt/C, potential excursions from the double layer region (0.54 V *vs.* RHE) to 0.0 V caused significant changes in the XAS spectra whereas none was observed for the alloys. The L_3 and L_2 x-ray absorption near edge structure indicated the generation of empty electronic states in the vicinity of the Fermi level due to adsorption of hydrogen, and the L_3 extended x-ray absorption fine structure indicated an increase in the coordination number of the first Pt-Pt shell from 9 to 11. The latter was attributed to a reversible surface restructuring process. Alloying of the Pt suppresses both the electronic and structural effects at 0.0 V. A comparison of the electrochemical kinetics for hydrogen oxidation by these electrocatalysts in a proton exchange membrane fuel cell indicated that alloying of the Pt had insignificant effects on the kinetics.

Previous work[1] has shown that the most accepted mechanism of hydrogen molecule oxidation is the Tafel-Volmer sequence, with the rate-determining step being dissociation of the hydrogen molecule (Tafel, Ref. 2) followed by a fast oxidation step (Volmer reaction). Despite the facile nature of this reaction on Pt and Pt group metals, a better understanding of the electrocatalysis in terms of the electronic and geometric parameters involved is essential. The primary motivation emanates from the promise of electrocatalysts with better tolerance toward commonly encountered catalyst poisons such as CO and S [3-5] and the eventual success of the direct methanol fuel cells.[6]

The electronic and geometric parameters which determine the electrocatalysis encompass several factors such as (*i*) the crystallite size effect, coordination numbers, bond distances, etc., and (*ii*) the Pt 5 d orbital vacancies. The effect of crystallite size and other geometric parameters for Pt has been extensively reviewed.[7,8] Attempts to understand the mechanism and kinetics of hydrogen molecule oxidation on Pt surfaces based on different models of hydrogen chemisorption and the interplay of electronic factors have also been made.[9-10]

The x-ray absorption spectroscopy (XAS) technique with the near edge part (x-ray absorption near edge structure, XANES) and higher energy side of the spectra (extended x-ray absorption fine structure, EXAFS) offers the prospect for investigating these factors and their interplay under *in situ* conditions of hydrogen oxidation. Recently we have completed an *in situ* XAS study on a series of carbon supported Pt alloy electrocatalysts, where Pt is alloyed with the first row transition elements (Cr, Mn, Fe, Co, and Ni).[11,12] This study correlated the electronic (Pt 5 d orbital vacancy obtained from the Pt L_3 and L_2 XANES) and geometric parameters (bond distance and coordination numbers from the Pt L_3 EXAFS) with electrocatalysis for oxygen reduction reaction (ORR).

There have been several reports on the effect of adsorbed hydrogen on the Pt L_3 XANES and the Pt d band vacancies. Almost all of these are for oxide-supported Pt catalysts in gaseous hydrogen.[13-14] The main effect is a broadening of the Pt L_3 XANES white line on the high energy side of the peak. Similar effects have been observed for carbon supported Pt electrodes in 1 *M* $HClO_4$ in the hydrogen adsorption region.[15] Boudart has attributed this widening of the white line to transitions into Pt-H antibonding orbitals.[14]

Recently Allen *et al.*, have used *in situ* dispersive EXAFS to study carbon supported Pt over a wide potential range.[16] They found significant increases in the magnitude of the first peak (the first Pt-Pt shell) of the Fourier

* Electrochemical Society Active Member.

transform in the hydrogen adsorption region. No explanation was given for this, but it indicates some structural changes. Tidswell *et al.*,[17] using x-ray reflectivity on Pt single crystals (<100>), have shown that adsorbed hydrogen can induce surface relaxation on Pt.

All these studies indicate that adsorbed hydrogen can induce significant electronic and structural changes on Pt. The implication of this for the hydrogen oxidation kinetics or the susceptibility of the electrode to poisons is not known. The present study uses *in situ* XAS to study electronic and structural changes in carbon supported Pt and Pt alloys in the hydrogen adsorption region.

Experimental

Electrocatalysts, electrodes, and electrochemical characterization.—Five carbon-supported binary Pt alloys (Pt/Cr, Pt/Mn, Pt/Fe, Pt/Co, and Pt/Ni) and Pt electrocatalysts were procured from Johnson Matthey Inc. (West Deptford, NJ). Based on previous investigations[18,19] the electrocatalyst loading was chosen as 20% (by weight) metal on carbon. The gas diffusion electrode structure comprised a reaction layer (containing 40 to 50% PTFE) and a wetproofed carbon cloth substrate (Textron, MA). The electrodes were prepared with a constant Pt loading of 0.3 mg/cm^2 (confirmed by atomic absorption spectroscopy).

The electrode kinetic evaluation of hydrogen oxidation was conducted at a solid polymer electrolyte membrane (SPEM) interface at 95°C and 5 atm pressure. Methodologies for electrode impregnation with Nafion® solution (Aldrich), membrane electrolyte purification (Aciplex,® Asahi Chemical Co., Japan), and the fabrication of the membrane electrode assembly (MEA) are described elsewhere.[20,21] The MEA was next incorporated into a single-cell test fixture with capabilities for half-cell measurements.[21] Electrode kinetic measurements were carried out in a test station with provisions for temperature and pressure control, humidification of reactant gases, and gas flow measurements.[21] Prior to electrode kinetic measurements, the MEA assembly was conditioned at several temperature, pressure, and humidity conditions, details of which are given elsewhere.[21] Besides the electrode kinetic measurements at 95°C and 5 atm pressure, measurements were also carried out as a function of temperature (in the range 35 to 80°C) for determination of the activation energy.

X-ray diffraction.—The characteristics of the crystalline structure of the supported Pt and Pt alloy electrocatalysts (formation of superlattices, etc.) were determined using x-ray powder diffraction (XRD). Measurements were carried out using a Sintag automated diffractometer with a Cu K_α radiation source. 2θ Bragg angle were scanned over a range of 0 to 80°. The diffraction patterns were recorded and analyzed by comparing them with standard powder diffraction data such as the JCPDS powder diffraction patterns (NIST). Details of sample preparation, internal calibration, and analysis are given elsewhere.[11,12]

In situ XANES and EXAFS investigation.—The x-ray absorption spectroscopic measurements were carried out at the National Synchrotron Light Source (NSLS), Brookhaven National Laboratory (BNL), using the National Institute of Science and Technology (NIST) beam line X23A2. Details of the monochromator design and energy resolution are given elsewhere.[11] Based on the monochromator and the overall beam line configuration, the presence of second harmonics was negligible. This was confirmed at both Pt (L_3 and L_2 edge) and the K edge of the alloying element using absorption edges of test samples at approximately twice the energy.[11]

Prior to electrode fabrication all the electrocatalysts were soaked in either 2 *M* KOH or 1 *M* $HClO_4$ to remove residual oxides and unalloyed first row transition elements. The electrodes used for the *in situ* XAS measurements were prepared by a vacuum table paper making technique[22] and comprise 76% electrocatalyst, 12% carbon fibers, and 12% PTFE (Teflon TFE-30, Du Pont). This afforded adequate step heights at both Pt L and the K edge of the alloying element in transmission and fluorescence modes. The electrodes were soaked in 1 *M* $HClO_4$ for 48 h to ensure complete wetting prior to incorporation in the spectroelectrochemical cell. Since XAS is an averaging technique, it was essential to ensure that all of the electrocatalyst was electroactive and there was a minimal amount of residual oxides and other phases (<5%). The spectro-electrochemical cell used as a part of this study allowed measurements in both transmission and fluorescence modes. The cell comprised the working electrode and an uncatalyzed carbon counterelectrode that were wetted with 1 *N* $HClO_4$. The separator used was a Nafion 117 proton exchange membrane (Du Pont). The reference was a calomel electrode, however, all potentials in the paper are reported *vs.* the reversible hydrogen electrode (RHE). The electrolyte was 1 *N* $HClO_4$, chosen due to nonabsorption of its anion, a property similar to that of the perfluorinated sulfonic acid membrane (Aciplex,® Asahi Chemical Company, Japan). The cell was specially constructed to maintain all components under compression in order to avoid complications in the spectra due to random density fluctuations caused as a result of gas bubbles. Details of the cell and the data acquisition setup are given elsewhere.[11,12] The potential control for the *in situ* XAS measurements was carried out using a potentiostat (Stonehart Associates, Model No. BC-1200) and a function generator (EG&G Princeton Applied Research Model No. PAR-175). XAS data were first recorded at the Pt L_2 and L_3 edges and then at the K edge of the respective alloying element. The measurements were first made at the open-circuit potential and then at potentials of 0.0, 0.24, and 0.54 V. The potential was changed from one value to the next at a sweep rate of 1 mV/s. The K edge XAS measurements for the alloying element were then carried out at 0.0, 0.24, 0.54, 0.84, and 1.14 V to check for the stability of the alloying element.

The methods used in analyzing the Pt XANES data and the determination of the Pt d band vacancies followed those of Mansour and co-workers[13,23] and are described in detail elsewhere.[11,12] The EXAFS data were analyzed by methods described in detail in previous publications.[11,12,24] Phase and amplitude data for the Pt-Pt and Pt-O interactions were derived from Pt foil and $Na_2Pt(OH)_6$ data at liquid nitrogen temperature. The FEFF program of Rehr *et al.*,[25] (version 4.08) was used to derive the Pt-M (M denotes the first row transition element) phase and amplitude parameters.

Results and Discussion

X-ray diffraction.—Comparison of the x-ray powder diffraction patterns with those of the standard JCPDS powder diffraction data base shows that the PtMn/C, PtCr/C, PtFe/C, PtCo/C, and PtNi/C alloys form intermetallic crystalline structures, the primary superlattice phase being of the type Pt_3M (where M is the first row transition alloying element) possessing an LI_2-type lattice with an fcc structure. There were indications of a small contribution of a secondary phase of the type PtM possessing an

Table I. Structural characteristics of the Pt and Pt alloy electrocatalysts, obtained from x-ray powder diffraction studies.

Electrocatalyst	Lattice parameter (Pt-Pt bond distance) (Å)	Average particle size (Å)
Pt/C	3.927 (2.777)	35
PtMn/C	3.898 (2.756)	69
PtCr/C	3.873 (2.738)	57
PtFe/C	3.866 (2.733)	58
PtCo/C	3.854 (2.725)	69
PtNi/C	3.812 (2.695)	58

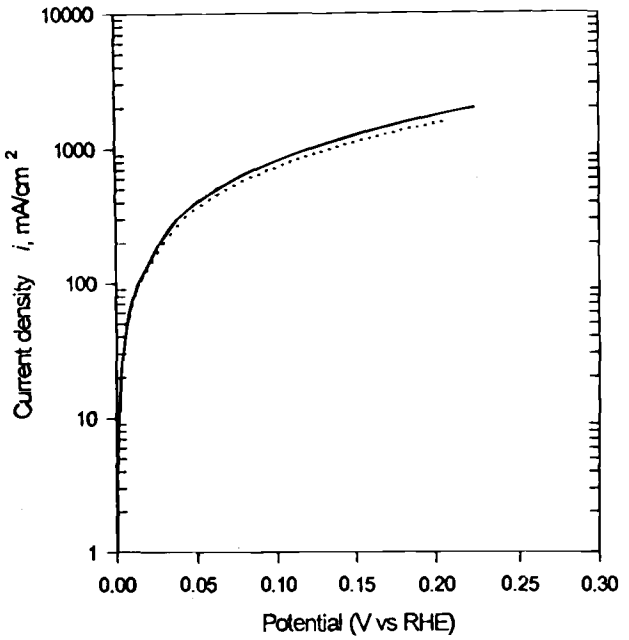

Fig. 1. Polarization curves for hydrogen oxidation on Pt and Pt alloy electrocatalysts in a proton exchange membrane fuel cell at 95°C and 5 atm pressure for Pt and Pt alloy electrocatalysts, Pt loading on electrodes, 0.3 mg/cm². PtCr/C (—) and Pt/C (···). Data for PtMn/C, PtFe/C, PtCo/C, and PtNi/C were almost identical to PtCr/C.

LI_o-type lattice with a tetragonal structure. The extent of contribution of this secondary phase (<5%), was estimated by the intensity of the diffraction lines due to the PtM phase. The 2θ positions of the <100>, <111>, <200>, and <220> powder diffraction lines for the Pt/C electrocatalysts compares well with the standard JCPDS powder diffraction files and indicates that the electrocatalyst Pt/C has fcc lattice similar to bulk Pt. The lattice parameters for the Pt alloys, based on the Pt_3M type fcc lattice (Table I), reveal contractions, in comparison to those for the Pt/C electrocatalyst. The lattice parameters decrease in the order Pt/C > PtMn/C > PtCr/C > PtFe/C > PtCo/C > PtNi/C (Table I). The particle sizes, based on x-ray line broadening, were estimated using the Scherrer equation[26] and the linewidth at half maximum intensity, corrected for instrument broadening, was obtained using Warrens equation.[27] The particle sizes were obtained from peak broadening of <111> diffraction line of the primary phase in the Pt and Pt alloys, relative to the <220> diffraction line for 20 μm spherical particles of Al powder (AESAR, Johnson Matthey) used as an internal standard (2θ peak position at 44.6°). Table I shows that particle size increases due to alloying in the order of Pt/C < PtCr/C < PtFe/C, PtNi/C < PtCo/C, PtMn/C.

Electrochemical characterization.—Figure 1 shows the Tafel plots for the Pt and Pt alloy electrocatalysts at 95°C and 5 atm pressure. The electrocatalytic activities for both Pt and Pt alloy electrocatalysts for hydrogen oxidation are almost identical.

Figure 2a shows the representative plot of the effect of temperature on the polarization behavior of PtCr/C. The rate constant for hydrogen dissociation (K_{at}) was derived from the limiting current (i_{Lim}) using a previously derived[3] expression

$$i_{Lim} = 2FA_iC^o_{H_2}(\gamma K_{at}D)^{1/2} \quad [1]$$

where A_i is the interfacial roughness; γ the active surface area per unit volume of porous electrode; D, the effective diffusivity of hydrogen in the electrolyte-filled reaction layer; and $C^o_{H_2}$, the concentration of hydrogen at the membrane electrolyte interface. The interfacial roughness factor A_i was taken as 2 (a reasonable value based on previous models[3,28,29]). The value of γ (Table II) was calculated as 0.96 to 1.23 × 10^8 cm^2 Pt/cm^3 (based on previously reported roughness factors,[11,12] a Pt loading of 0.3 mg/cm^2, and a penetration depth of 10 μm (based on previously reported Rutherford backscattering results[30]). The diffusivity of hydrogen and its dependence on the hydrogen concentration at the electrolyte-reaction layer interface were obtained from previously published values.[31,32] The temperature dependence of the rate constant for hydrogen dissociation (K_{at}) was used to derive a measure of the activation energy ΔH_{act}. Figure 2b shows an Arrhenius plot for the PtCr/C electrocatalyst, and the values of activation energies are given in Table II. There was no variation in the activa-

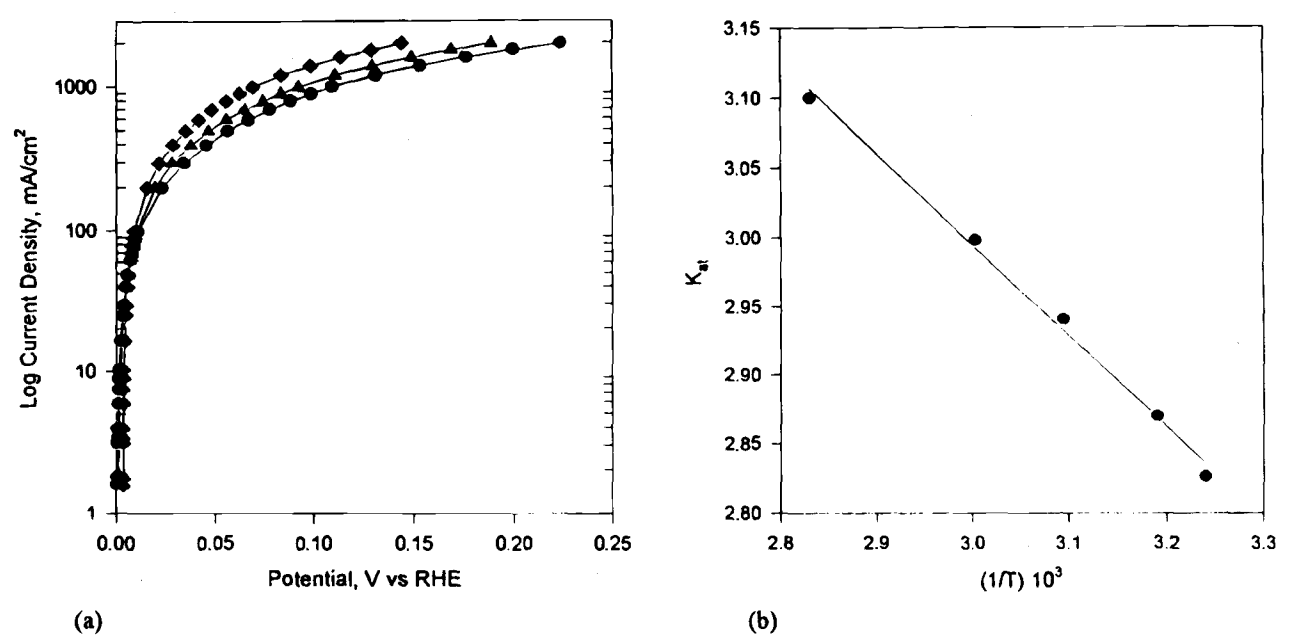

Fig. 2. Behavior of a PtCr/C electrocatalyst in terms of (a) variation in hydrogen polarization as a function of temperature, [30 (●), 50 (▲), and 80°C (◆)] and (b) the corresponding Arrhenius plot.

Table II. Electrochemical kinetic parameters for hydrogen oxidation.

Electrocatalyst	γ (10^4 cm^{-1})	ΔH_{act} (KJ/mol)	(θ_o)
Pt/C	1.22	10.88	0.95
PtCr/C	1.01	9.62	0.95
PtMn/C	0.96	10.04	0.94
PtFe/C	1.12	10.46	0.95
PtCo/C	0.98	10.46	0.89
PtNi/C	0.96	9.83	0.88

(γ) Active surface area per unit volume of porous electrode.
(θ_o) Surface coverage by hydrogen.

tion energies, indicating a similar Tafel-Volmer mechanism for Pt and Pt alloys. This agrees with previously published results for PtRh and PtRu alloys.[33]

The hydrogen coverage (θ_o) was derived by fitting the normalized polarization data to the expression[3]

$$I/I_{Lim} = (1 - \theta_o)\,\frac{1 - e^{-2F\eta/RT}}{1 - \theta_o(1 - e^{-F\eta/RT})} \qquad [2]$$

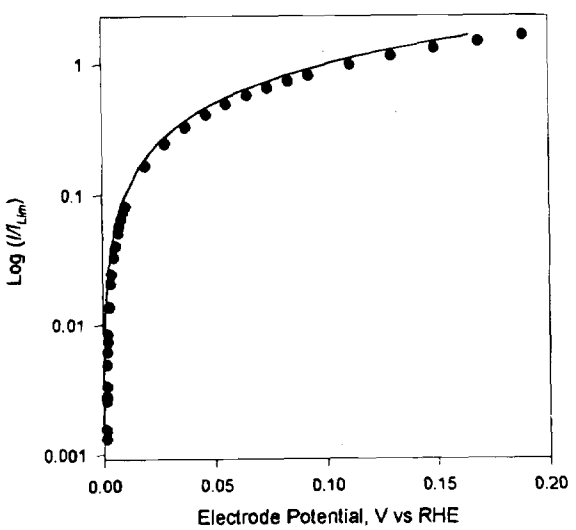

(a)

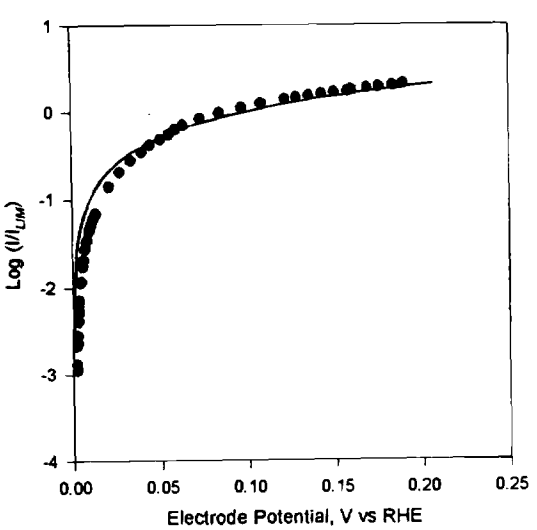

(b)

Fig. 3. Fit between the theoretically derived polarization curve (—) using (θ_o = 0.95) and the experimental data at 60°C for (a) PtCr/C and (b) Pt/C electrocatalysts.

Table III. Percent atomic ratio of Pt to alloying element and electronic parameters (Pt 5 d orbital vacancy) for Pt and Pt alloy electrocatalysts as obtained from *in situ* XANES analysis at 0.0 and 0.54 V *vs.* RHE.

Electrocatalyst	Atom Percent (Pt: alloying element)	0.0 V $(h_J)_{t,s}$[a]	0.54 V $(h_J)_{t,s}$[a]
Pt/C	—	0.335	0.329
PtCr/C	—	0.359	0.360
PtMn/C	64.17	0.333	0.331
PtFe/C	68.10	0.370	0.368
PtCo/C	64.60	0.398	0.400
PtNi/C	76.45	0.410	0.412

[a] $(h_J)_{t,s}$ denotes the Pt 5 d orbital vacancy per atom.

Figure 3 shows fits for the PtCr/C and Pt/C data at 60°C. The results for Pt and Pt alloys are given in Table II. The hydrogen coverages do not differ significantly between the supported Pt and Pt alloy electrocatalysts and may indicate that the outer surface of the Pt alloys is mostly Pt. In binary alloys, with a Pt_3M stoichiometry, and an LI_2 crystal structure, it is possible to have surface enrichment without surface segregation as has been reported for Pt/Ti, [34] Pt/Co, [35] Pt/Sn, [36] and Pt/Ni alloys.[37]

XAS analysis.—The alloy composition was calculated from the respective edge jumps at Pt L_3 and K edges of the alloying elements and the absorption cross sections obtained from the McMaster Tables[38] and the results (Table III) agree with a Pt_3M stoichiometry.[39,40]

XANES analysis.—Figure 4a shows the *in situ* Pt L_3 XANES for a Pt foil and a Pt/C electrocatalyst at 0.0 and 0.54 V *vs.* RHE. At 0.0 V there is considerable widening of the white line on the high energy side of the peak. This effect is completely reversible with potential. At 0.54 V (double layer region) the spectra for Pt/C is identical to that for a Pt foil which indicates that there is no interference due to anion or water adsorption. Such a widening of the white line in the hydrogen region is similar to that previously reported in the gas-phase studies on oxide supported Pt catalysts by Mansour and co-workers[13,23] and by Samant and Boudart.[14] Samant and Boudart[14] have presented their results as the difference spectra relative to a Pt foil. Similar plots are shown in Fig. 4b. Negative difference spectrum indicate features present in the Pt foil that are absent in the electrocatalyst sample. The features at ~18 eV and above correspond to the first oscillation beyond the white line, and hence the presence of this feature in the difference spectrum can be attributed to the change in coordination number of Pt in going from bulk (foil) to small supported crystallites. At energies below 18 eV, the difference spectra reflect changes in the electronic structure of Pt. In the hydrogen region (0.0 V), there is a major positive feature at ~9 eV. This suggests the formation of unoccupied states on the high energy side of the Fermi level of Pt. Calculation of the 5 d orbital vacancies using the areas under the L_3 and L_2 white lines (details of the methodology given elsewhere[11,12,23]) at 0.0 and 0.54 V reflect these observations (Table III), which support the earlier suggestion[14] of the creation of antibonding states above the Fermi level of Pt due to hydrogen adsorption.

A similar comparison in the case of Pt alloys (Fig. 5a shows representative XANES for PtNi/C) shows that alloying causes an increase in the white line thereby indicating higher d band vacancy of Pt. This is exhibited by the increased magnitude of the white line for PtNi/C at 0.54 V (Fig. 5a). Further, there appears to be no appreciable differences in the white lines at 0.0 and 0.54 V, indicating minimal change in the electronic structure of Pt in the alloys at the hydrogen region. These observations are quantitatively reflected in the calculated d band vacancies (Table III). The corresponding difference spectrum (Fig. 5b) clearly indicates the minimal change in electronic structure of Pt in the hydrogen region in contrast to the

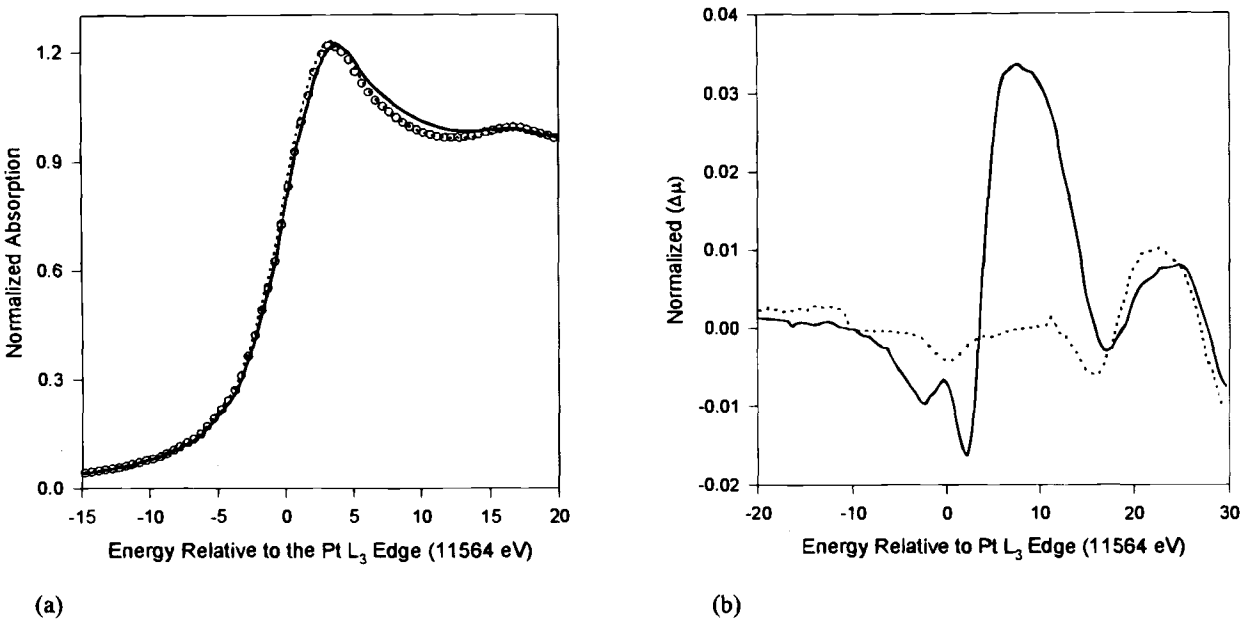

Fig. 4. (a) Pt L_3 XANES spectra for a Pt foil (O) and for a Pt/C electrocatalyst in 1 *M* $HClO_4$ at 0.0 V (—) and 0.54 V (···). (b) Difference spectra at 0.0 (—) and 0.54 V (···).

Pt/C electrocatalyst. The negative feature at ~18 eV is similar to those observed for the Pt/C electrocatalyst and can be attributed to the smaller crystallite size of the sample. The positive feature at 9 eV corresponds to the increased Pt 5 d orbital vacancy as a result of alloying.

XANES analysis at the alloying element K edge in the potential region of 0.54, 0.84, and 1.14 V have been reported previously.[11,12] These previous results have shown no evidence of any redox-type process involving the alloying element as well as negligible corrosion even at potentials above 0.8 V *vs.* RHE. These results strongly indicate that the outer surface is mostly Pt.

EXAFS analysis.—EXAFS spectra at the Pt L_3 edge were used to investigate the effect of potential on the short range atomic order (bond distances, coordination number, and Debye Waller factor) of Pt and Pt alloys. Figure 6 shows the representative plots for the isolated EXAFS at the Pt L_3 edge for Pt/C at 0.0 V. Table IV gives the integration range in k space for the forward Fourier transforms. Comparison of the Fourier transforms at 0.0 and 0.54 V for Pt/C electrocatalysts is shown in Fig. 7. Once again the effect of potential in the EXAFS is reversible. The higher magnitude of Fourier transform at 0.0 V indicates a significant change in the structural parameters for the Pt/C electrocatalyst in the hydrogen region relative to the double layer (0.54 V). This observation of a higher magnitude of the Fourier transform is in agreement with previously reported *in situ* results on a supported Pt/C electrocatalyst.[16] A corresponding analysis for the Pt alloys, as shown by the representative plots for PtMn/C and PtNi/C (Fig. 8), however, shows minimal changes with potential.

The increase in the magnitude of the first peak in the Fourier transform can be attributed to changes in the Pt-Pt coordination number (N), changes in the Debye Waller

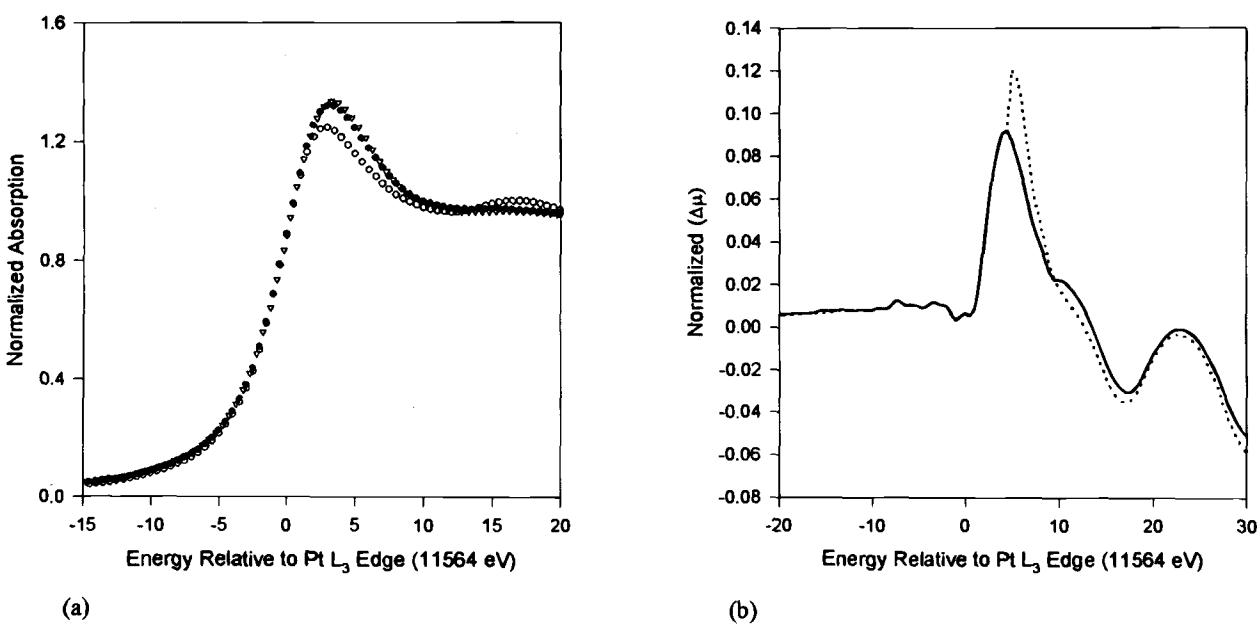

Fig. 5. (a) Pt L_3 XANES spectra for a Pt foil (O) and for a PtNi/C electrocatalyst in 1 *M* $HClO_4$ at 0.0 V (●) and 0.54 V (▽). (b) Difference spectra at 0.0 (—) and 0.54 V (···).

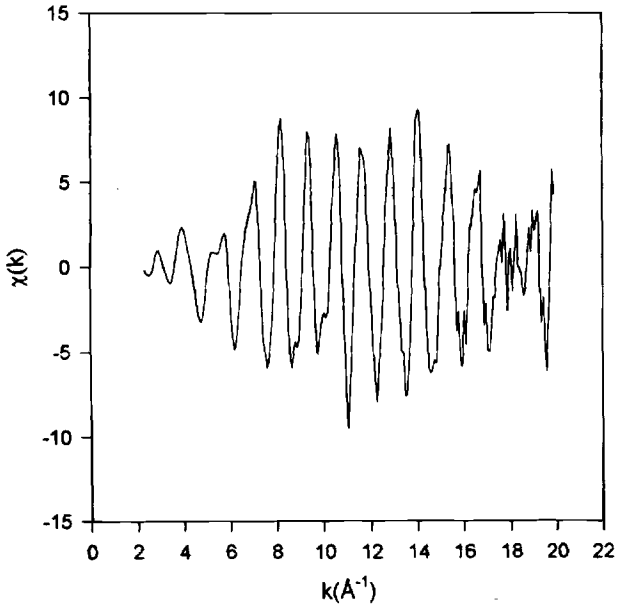

Fig. 6. EXAFS spectrum at the Pt L_3 edge for Pt/C electrocatalyst at 0.0 V.

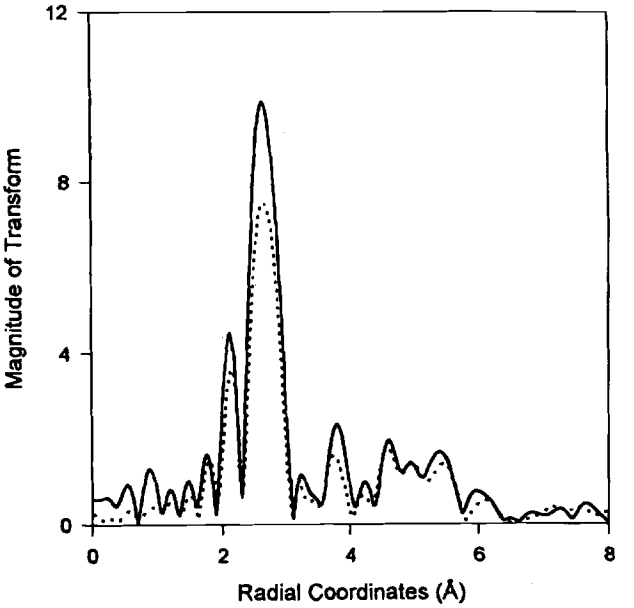

Fig. 7. Comparison of Fourier transform (k^3 weighted) at 0.0 (—) and 0.54 V (···) *vs.* RHE for Pt/C electrocatalyst (Δk values in Table IV).

factor ($\Delta\sigma^2$), the introduction of another coordination shell (*e.g.*, Pt-C), or to forward scattering effects due to hydrogen in the Pt lattice. The presence of extra coordination shells and the forward scattering were checked by doing Pt-Pt phase corrected Fourier transforms on the data. In all cases, the peak of the real part of the Fourier transform coincided with a symmetrical positive peak in the imaginary part of the transform. This is evident from Fig. 9, showing such a comparison at 0.0 V. This indicates a single Pt-Pt coordination shell, and it eliminates forward scattering as an explanation of the higher peak. Extra coordination shells would introduce asymmetry in the main peak of the imaginary part of the transform. Forward scattering would change the phase and the maxima would not coincide. The effects of N and $\Delta\sigma^2$ were separated by comparing k^1 and k^3 weighted fits[41] and by use of the log ratio method.[42,43] For the log ratio test the log ratio of the amplitudes for the Pt reference foil and the Pt/C were plotted *vs.* k^2. The intercept at $k = 0$ Å^{-1} yields the coordination number and the slope of the line, $\Delta\sigma^2$. This yielded $N = 10.7$ and $\Delta\sigma^2 = 0.0046$ for the Pt/C at 0.0V and $N = 8.7$ and $\Delta\sigma^2 = 0.0045$ at 0.54 V. This indicated that the changes in the EXAFS are due mainly to changes in the coordination number at 0.0 V.

Detailed EXAFS analysis was performed after obtaining the inverse Fourier transforms and performing fits with phase and amplitude data that were either derived experimentally (Pt foil at liquid N_2 temperature for the Pt-Pt phase and amplitude parameters) or theoretically (FEFF program, for the Pt-M phase and amplitude parameters). All fits were performed using iterative least square fitting.[44] All relevant parameters for the forward and inverse Fourier transforms for the sample and reference standards are given in Table IV. The approach taken in fitting the sample data was to choose the simplest model first and attempt to get unique solutions to the fits. Thus for Pt/C electrocatalyst it was possible to fit the data to a

Table IV. Fourier transformation ranges of the forward and inverse transforms (k^3 weighted) for Pt and Pt alloy electrocatalysts at 0.0 and 0.54 V *vs.* RHE.

	0.0 V *vs.* RHE		0.54 V *vs.* RHE	
Electrocatalyst	Δk (Å^{-1})	Δr (Å)	Δk (Å^{-1})	Δr (Å)
Pt/C	3.53 to 14.31	1.41 to 3.41	3.49 to 14.23	1.40 to 3.05
PtCr/C	3.30 to 14.50	1.41 to 3.41	3.15 to 14.71	1.41 to 3.41
PtMn/C	3.54 to 14.45	1.40 to 3.32	3.70 to 14.22	1.21 to 3.61
PtFe/C	3.28 to 14.51	1.5 to 3.31	3.45 to 14.74	1.50 to 3.40
PtCo/C	3.20 to 14.48	1.38 to 3.41	3.22 to 14.61	1.50 to 3.50
PtNi/C	3.25 to 14.20	1.50 to 3.50	3.55 to 14.64	1.50 to 3.50

Fourier transformation ranges of the foward aznd inverse transforms for reference standards.

Reference standard	Δk (Å^{-1})	Δr (Å)	N_{ref}	R_{ref}
Pt foil (liquid N_2 temperature) (Pt-Pt standard)	3.55 to 19.22	1.04 to 3.52	12	2.774
Pt-Cr standard (FEFF program)	3.30 to 19.50	1.40 to 3.10	12	2.774
Pt-Mn standard (FEFF program)	3.30 to 19.45	1.40 to 2.92	12	2.774
Pt-Fe standard (FEFF program)	3.14 to 18.14	1.45 to 2.95	12	2.774
Pt-Co standard (FEFF program)	2.92 to 19.17	1.40 to 3.40	12	2.774
Pt-Ni standard (FEFF program)	2.55 to 19.25	1.50 to 3.50	12	2.774

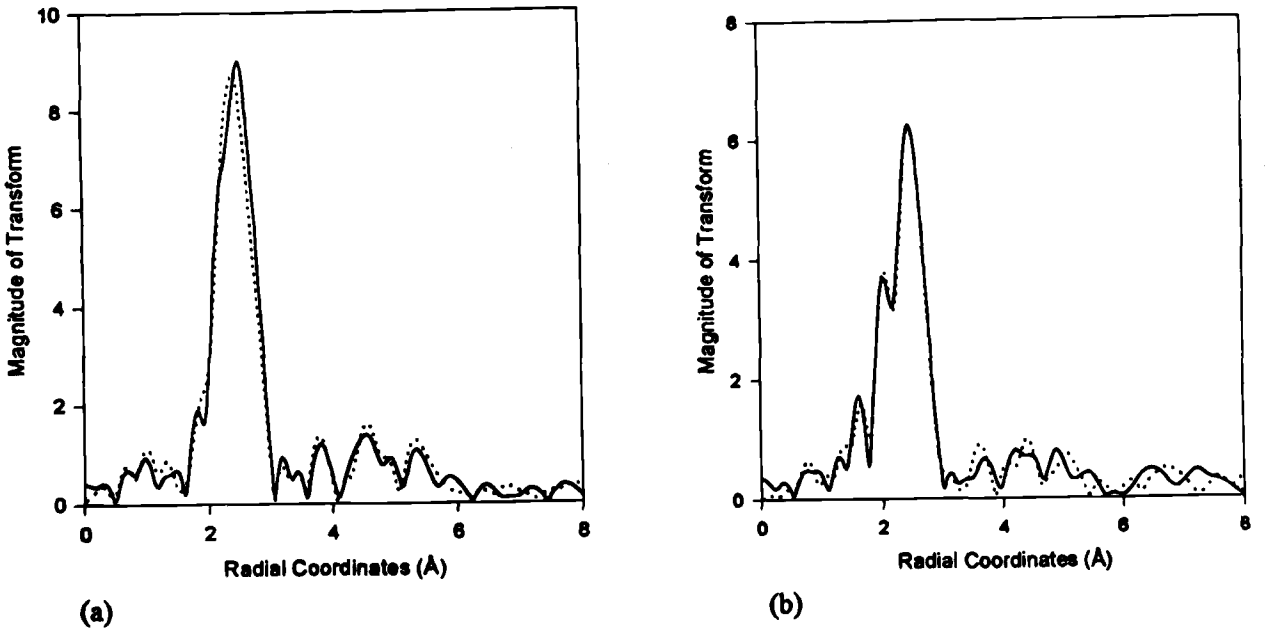

Fig. 8. Comparison of Fourier transform (k^3 weighted) at 0.0 (—) and 0.54 V (···) *vs.* RHE for (a) PtMn/C and (b) PtNi/C electrocatalyst (Δk values in Table IV).

single Pt-Pt coordination shell at both 0.0 and 0.54 V. Figure 10 shows the quality of this fit at 0.0 V in both k and r space. Similarly the Pt alloy data were fitted to a two-shell model consisting of Pt-Pt and Pt-M contributions at both the potentials. The quality of fits obtained is shown by the representative plots for PtCr/C alloy at 0.54 V (Fig. 11) in both k and r space. The results of EXAFS analysis are given in Tables V and VI. The error limits in the EXAFS analysis were obtained according to procedure described elsewhere.[45] For single shell fits, the limits of error ranged between 1 and 8% for N and 0.005 to 0.01 Å for R. For two shell fits, the error limits were typically in the range of 5 to 14% for N and 0.007 to 0.012 Å for R. The single shell fits are more reliable than two shell fits, since they can be verified using the log ratio method. This could account for some of the variation in the total coordination numbers for the alloys.

The results in Table V are in close agreement with those obtained using the log ratio method, confirming that there is an increase in the coordination number at 0.0 V as compared to 0.54 V. Further, the quality of fits obtained using k^1 weighting was of similar high quality and the values of the EXAFS parameters were essentially the same. These results strongly suggest restructuring of the Pt particles in Pt/C at the hydrogen region. Previous results of Tidswell *et al.*,[17] using x-ray reflectivity at the <100> Pt/electrolyte interface has shown that surface relaxation of Pt occurs on adsorption of hydrogen. Similar results have also been previously reported in vacuum interface studies using Rutherford backscattering at the <001> Pt surface.[46] Recent results by Zei *et al.*,[47] using *in situ* STM on <100> Pt surface have shown that a reconstructed <100> Pt surface ([5 × 20] symmetry, prepared using flame annealing) can be maintained on transfer to the electrolyte at negative potentials. Excursion to positive potentials lifts this reconstruction ([5 × 20] → [1 × 1]). However, unlike Au[48] there was no evidence of any reconstruction on going back to negative potentials. An explanation of the present results is that on the small supported Pt electrocatalyst particles such a reconstruction is possible and is reversible with potential. The reconstruction could change the particle shape and hence the coordination number. The coordination numbers at 0.0 V are what one would expect for a 25 Å particle with a cubo-octahedral structure. The lower coordination number at 0.54 V would indicate a different shape, perhaps a flat raft-like structure on the carbon support.

Results of the EXAFS analysis for the Pt alloy electrocatalysts at 0.0 and 0.54 V are given in Table VI. All the alloys exhibit contractions in their Pt-Pt distances confirming the results from the *ex situ* x-ray diffraction analysis. In contrast to the Pt/C electrocatalyst, there is no variation in the N, R, and $\Delta\sigma^2$ values for any of the alloy electrocatalysts with potential. This indicates that the process of alloying renders the electrocatalysts immune to structural changes in the hydrogen region. It is also important to consider the particle size difference between the supported Pt and the Pt alloy electrocatalysts. The particle sizes determined using x-ray line broadening analysis (Table I) indicates that compared to 35 Å for Pt/C the alloys have values ranging from 57 to 69 Å. Particle sizes determined from coordination numbers around Pt in Pt/C and Pt alloys (sum of Pt-Pt and Pt-M) using cubo-octahe-

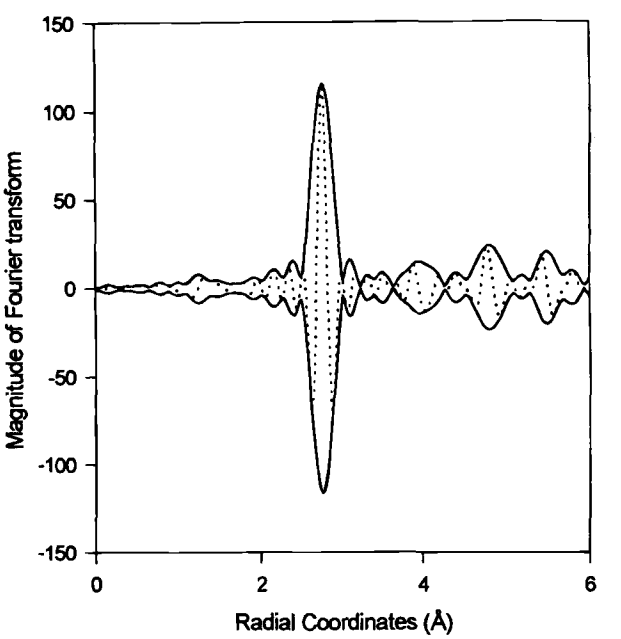

Fig. 9. Comparison of real (—) and imaginary (···) parts of the Fourier transform for Pt/C electrocatalyst at 0.0 V. The transform is Pt-Pt phase corrected and k^3 weighted; Δk = 3.0 to 18.0 Å^{-1}.

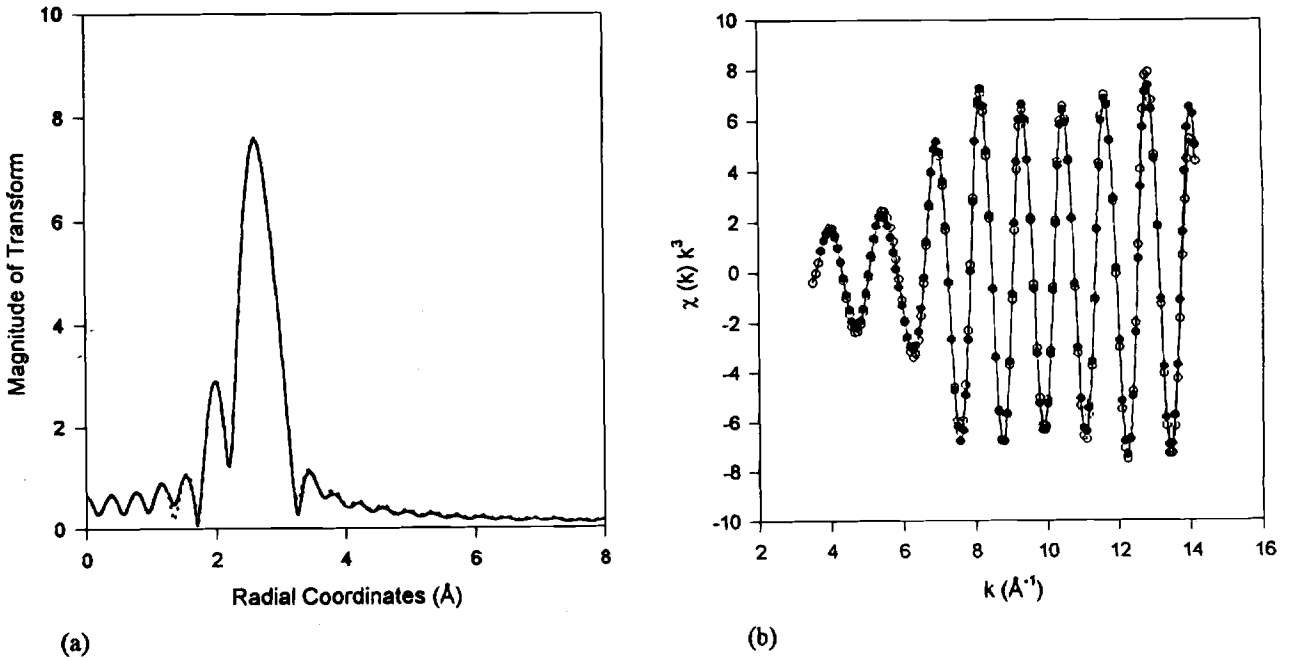

Fig. 10. Single shell fit for Pt/C electrocatalyst at Pt L_3 edge (0.0 V) in (a) r space and (b) k space. The fits are k^3 weighted with the sample data denoted by (···) in r and (○) in k space and the fitted data by (—) in r and (●) k space.

dral model for face centered cubic (fcc) clusters indicate slightly smaller particle sizes, ~25 Å for Pt/C and 40 to 55 Å for the Pt alloys.[49] The percent ratio of surface atoms to the total number of atoms (N_S/N_t) changes from 28 to 20% in going from 25 to 70 Å. The decrease in N_s/N_t in going from Pt/C to the alloy catalyst is not enough to account for the absence of effects on the XAS of the alloys in the hydrogen region. Thus the differences between the behavior of the Pt/C and the Pt alloy electrocatalysts cannot be attributed to a trivial particle size effect. The shorter Pt-Pt bond distance in the alloy is also indicative of a more stable configuration that resists reconstruction at negative potentials. The Pt 5 d band vacancies for the alloys and the Pt-Pt bond distances show a smooth inverse relationship. However the increase in 5 d band vacancies at 0.0 V did not result in a contraction of the Pt-Pt bond distances. In acids with strongly adsorbing anions such as sulfate or phosphate, there is also an increase in the Pt L_3 edge white line without any modification of the Pt-Pt bond length. Apparently, empty states due to adsorbates such as hydrogen or anions do not affect Pt-Pt bonding, whereas the empty states due to alloying affect the Pt-Pt bond length. The Pt XANES for the alloys at 0.0 V indicates that there is no effect due to adsorbed hydrogen. Alloying may reduce the hydrogen adsorption. In case of Pt/C adsorption of hydrogen aids the reconstruction. The reconstruction on the Pt/C may cause a variation in the kinetic parameters for hydrogen oxidation with potential.

Table V. Results of *in situ* EXAFS analysis on the carbon supported Pt electrocatalyst at 0.0 and 0.54 V *vs.* RHE.

Electrode potential: 0.0 V.

$(h_j)_{t,s}$	Coordination shell	N	R (Å)	$\Delta\sigma^2$ (Å²)	ΔE_o
0.335	Pt-Pt	10.64	2.772	0.0044	0.93

Electrode potential: 0.54 V.

$(h_j)_{t,s}$	Coordination shell	N	R (Å)	$\Delta\sigma^2$ (Å²)	ΔE_o
0.329	Pt-Pt	8.66	2.773	0.0044	−0.88

This could account for the poorer fit for the kinetic data in Fig. 3b.

Conclusions

In summary, this study indicates that in contrast to the oxygen reduction reaction,[11,12] the electrocatalytic activities for hydrogen oxidation in Pt and Pt alloys do not differ significantly. Further, the mechanism for hydrogen oxidation appears to be same for both Pt and Pt alloy electrocatalysts as indicated by the similarity of their respective activation energies. The hydrogen coverages on all the Pt alloys were also found to be similar to the Pt/C

Table VI. Results of *in situ* EXAFS analysis on the carbon supported Pt electrocatalysts at 0.0 and 0.54 V *vs.* RHE.

Electrode potential: 0.0 V.

Electrocatalyst	Coordination shell	N	R (Å)	$\Delta\sigma^2$ (Å²)	ΔE_o
PtCr/C	Pt-Pt	8.45	2.70	0.0051	4.44
	Pt-Cr	2.73	2.68	0.0061	−6.16
PtMn/C	Pt-Pt	6.84	2.76	0.0045	3.20
	Pt-Mn	2.98	2.69	0.0024	−6.81
PtFe/C	Pt-Pt	6.62	2.71	0.0032	4.96
	Pt-Fe	2.82	2.65	0.0042	−5.77
PtCo/C	Pt-Pt	7.14	2.67	0.0071	7.51
	Pt-Co	2.41	2.64	0.0061	−11.45
PtNi/C	Pt-Pt	8.81	2.70	0.0046	2.45
	Pt-Ni	2.64	2.62	0.0074	−9.09

Electrode potential: 0.54 V.

Electrocatalyst	Coordination shell	N	R (Å)	$\Delta\sigma^2$ (Å²)	ΔE_o
PtCr/C	Pt-Pt	8.53	2.71	0.0066	5.20
	Pt-Cr	2.78	2.69	0.0039	−7.58
PtMn/C	Pt-Pt	7.52	2.76	0.0057	1.04
	Pt-Mn	2.75	2.68	0.0023	−8.11
PtFe/C	Pt-Pt	6.71	2.70	0.0034	9.45
	Pt-Fe	2.98	2.64	0.0065	−6.51
PtCo/C	Pt-Pt	6.94	2.68	0.0057	5.48
	Pt-Co	2.48	2.63	0.0061	−8.37
PtNi/C	Pt-Pt	9.12	2.68	0.0072	7.55
	Pt-Ni	2.72	2.61	0.0114	−9.12

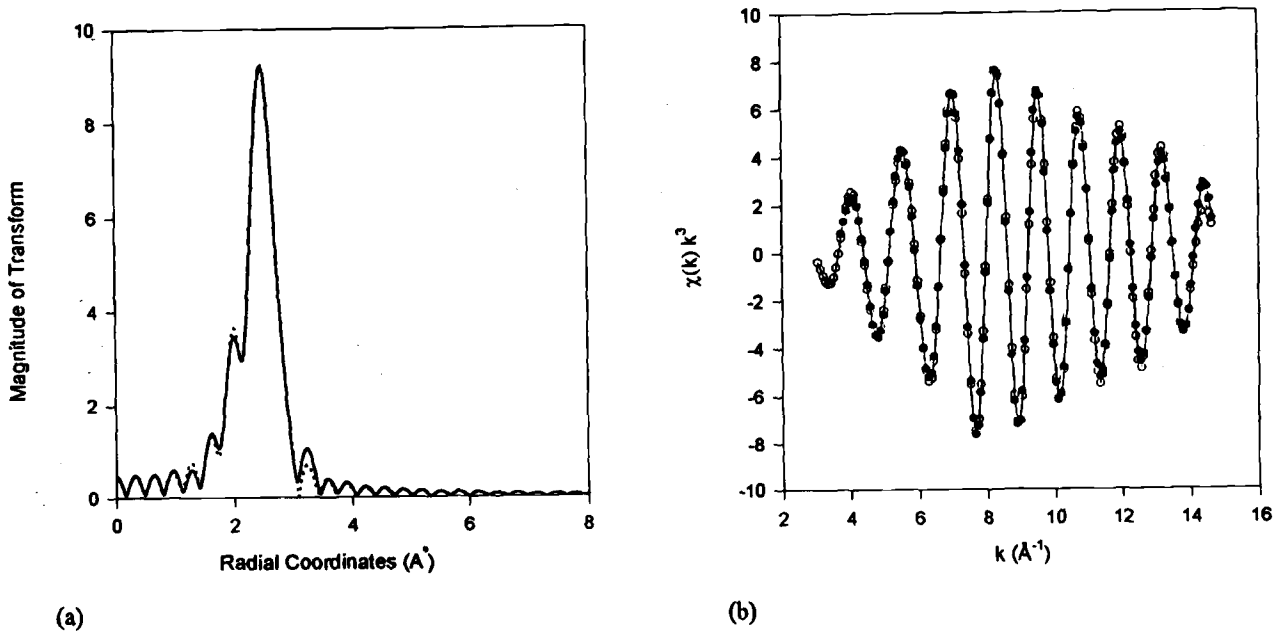

Fig. 11. Two shell fit for PtCr/C electrocatalyst at Pt L_3 edge (0.0 V) in (a) r space and (b) k space. The fits are k^3 weighted with the sample data denoted by (···) in r and (○) in k space and the fitted data by (—) in r and (●) k space.

electrocatalyst. This implied that the outer surface of the electrocatalyst particles is mostly Pt.

XAS analysis revealed that all the alloys possessed higher Pt 5 d band vacancies per atom as compared to the Pt/C electrocatalyst. They also confirmed results of x-ray diffraction that alloying caused contraction of the lattice parameters. In the case of the Pt/C electrocatalyst, the Pt 5 d band vacancies were higher at 0.0 V as compared to 0.54 V, indicating that the H adsorption at 0.0 V resulted in increased d band vacancies. These electronic changes were associated with a change in the Pt-Pt coordination numbers, with higher N values at 0.0 V as compared to 0.54 V (all other parameters remained unchanged, *i.e.*, R and $\Delta\sigma^2$). This is attributed to a reversible reconstruction effect which changes the particle shape. In contrast to this, the Pt alloy electrocatalysts showed no influence of potential on either the d band vacancies or the structural parameters.

Acknowledgments

The authors gratefully acknowledge the support of the U.S. Department of Energy, Division of Material Science, Brookhaven National Laboratory (Contract No. DEA-CO2-76CH00016) for its role in the development and operation of the National Synchrotron Light Source (NSLS). The help of NIST personnel at the Beam Line X23A2 in particular Joe Woicik and John Kirkland is gratefully acknowledged. The authors gratefully acknowledge Lindsay Keck of Johnson Matthey Inc., who supplied the electrocatalysts. The experimental work at Brookhaven was supported by the Office of Transportation Technologies, Electric and Hybrid Vehicles Division of D.O.E under Contract No. DEA-CO2-76CH00016.

Manuscript submitted Aug. 2, 1995; revised manuscript received April 4, 1996.

Brookhaven National Laboratory assisted in meeting the publication costs of this article.

REFERENCES

1. P. N. Ross and P. Stonehart, *J. Res. Inst. Catal., Hokkaido Univ.*, **22**, 22 (1974).
2. K. J. Vetter, *Electrochemical Kinetics*, p. 39, Academic Press, Inc., New York (1967).
3. W. Vogel, J. Lundquist, P. N. Ross, and P. Stonehart, *Electrochim. Acta*, **20**, 79 (1975).
4. H. P. Dhar, L. G. Christner, A. K. Kush, and H. C. Maru, *This Journal*, **133**, 1574 (1986).
5. D. T. Chin and P. D. Howard, *ibid.*, **133**, 2447 (1986).
6. P. N. Ross, *Electrochim. Acta.*, **36**, 2053 (1991).
7. S. Mukerjee, *J. Appl. Electrochem.*, **20**, 537 (1990).
8. K. Kinoshita, in *Modern Aspects of Electrochemistry*, Vol. 14, J. O'M. Bokris, B. E. Conway, and R. E. White, Editors, p. 557, Wiley, New York (1982).
9. R. Lewis and R. Gomer, *Surf. Sci.*, **17**, 333 (1969).
10. G. C. Bond, *Catalysis by Metals*, p. 162, Academic Press, Inc., New York (1962).
11. S. Mukerjee, S. Srinivasan, M. P. Soriaga, and J. McBreen, *This Journal*, **142**, 1409 (1995).
12. S. Mukerjee, S. Srinivasan, M. P. Soriaga, and J. McBreen, *J. Phys. Chem.*, **99**, 4577 (1995).
13. A. N. Mansour, J. W. Cook, Jr., D. E. Sayers, R. J. Emrich, and J. R. Katzer, *J. Catal.*, **89**, 464 (1984).
14. M. G. Samant and M. Boudart, *J. Phys. Chem.*, **95**, 4070 (1991).
15. J. McBreen and S. Mukerjee, Abstract 482, p. 743, The Electrochemical Society Meeting Abstracts, Vol. 95-1, Reno, NV, May 21-26, 1995.
16. P. G. Allen, S. D. Conradson, M. S. Wilson, S. Gottesfeld, I. D. Raistrick, J. Valerio, and M. Lovato, *Electrochim. Acta.*, **39**, 2415 (1994).
17. I. M. Tidswell, N. M. Markovic, and P. N. Ross, *Phys. Rev. Lett.*, **71**, 1601 (1993).
18. E. A. Ticianelli, C. R. Derouin, and S. Srinivasan, *J. Electroanal. Chem.*, **251**, 275 (1988).
19. S. Srinivasan, E. A. Ticianelli, C. R. Derouin, and A. Redondo, *J. Power Sources*, **22**, 359 (1988).
20. S. Mukerjee, S. Srinivasan, and A. J. Appleby, *Electrochim. Acta.*, **38**, 1661 (1993).
21. A. Parthasarathy, S. Srinivasan, and A. J. Appleby, *J. Electroanal. Chem.*, **339**, 101 (1992).
22. J. McBreen, W. E. O'Grady, K. I. Pandya, R. W. Hoffman, and D. E. Sayers, *Langmuir*, **3**, 428 (1987).
23. A. N. Mansour, Ph.D. Thesis, Dept. of Physics, University of North Carolina, Raleigh, NC (1983).
24. K. I. Pandya, W. E. O' Grady, D. A. Corrigan, J. McBreen, and R. W. Hoffman, *J. Phys. Chem.*, **94**, 21 (1990).
25. J. J. Rehr, J. Mustre de Leon, S. I. Zabinski, and R. C. Albers, *J. Am. Chem. Soc.*, **113**, 5135 (1991).
26. H. Klug and L. Alexander, *X-Ray Diffraction Procedures*, p. 491, Wiley, New York (1962).
27. L. V. Azaroff, *Elements of X-Ray Crystallography*, p. 556, McGraw Hill, New York (1968).
28. J. Giner and C. Hunter, *This Journal*, **116**, 1124 (1969).
29. R. P. Ickowski and M. B. Cutlip, *ibid.*, **127**, 1433 (1980).
30. J. G. Beery, E. A. Ticianelli, and S. Srinivasan, *J. Appl. Electrochem.*, **21**, 597 (1991).
31. R. S. Yeo and J. McBreen, *This Journal*, **126**, 1682 (1979).

32. M. W. Verbrugge and R. F. Hill, *ibid.*, **137**, 1131 (1990).
33. P. N. Ross, K. Kinoshita, A. J. Scarpellino, and P. Stonehart, *J. Electroanal. Chem.*, **63**, 97 (1975).
34. U. Bardi, D. Dahlgren, and P. N. Ross, *J. Catal.*, **100**, 196 (1986).
35. U. Bardi, B. Beard, and P. N. Ross, *ibid.*, **124**, 22 (1990).
36. A. Hanner and P. N. Ross, *J. Phys. Chem.*, **95**, 3740 (1991).
37. Y. Gauthier, I. Joly, R. Baudoing, and I. Rundgren, *J. Phys. Rev.*, **B31**, 6216 (1985).
38. W. H. Master, N. Kerr del Grande, J. H. Mallett, and J. H. Hubbel, *Compilation of X-Ray Cross Sections*, National Technical Information Service, Springfield, VA (1969).
39. C. Leroux, M. C. Cadaville, V. Pierron-Bohnes, G. Inden, and F. Hinz, *Phys. F: Met. Phys.*, **18**, 2033 (1988).
40. T. B. Massalski and H. Okamoto, *Binary Alloy Phase Diagrams*, ASM International, Materials Park, OH (1990).
41. D. C. Koningsberger, in *Synchrotron Techniques in Interfacial Electrochemistry*, C. A. Melendres and A. Tadjeddine, Editors, p. 181, Kluwer Academic Publishers, Dordrecht (1994).
42. E. A. Stern, D. E. Sayers, and F. W. Lytle, *Phys. Rev.*, **B11**, 4836 (1975).
43. F. W. Lytle, D. E. Sayers, and E. A. Stern, *ibid.*, **B11**, 4825 (1975).
44. G. H. Via, J. H. Sinfelt, and F. W. Lytle, *J. Chem. Phys.*, **71**, 690 (1979).
45. B. K. Teo, *EXAFS: Basic Principles and Data Analysis, Inorganic Chemistry Concepts 9*, p. 132, Springer Verlag, Heidelberg (1986).
46. J. A. Davies, T. E. Jackson, D. P. Jackson, and P. R. Norton, *Surf. Sci.*, **109**, 20 (1981).
47. M. S. Zei, N. Batina, and D. M. Kolb, *Surf. Sci. Lett.*, **306**, L519 (1994).
48. B. M. Ocko, J. Wang, A. Davenport, and H. Isaacs, *Phys. Rev. Lett.*, **65**, 1466, (1990).
49. R. B. Greegor and F. W. Lytle, *J. Catal.*, **63**, 476 (1980).

Topographic Changes of Polycrystalline Ag and Cu Electrodes in Acid Aqueous Solutions Resulting from a Prolonged Application of the Potential Reversal Technique

P. Carro,[a] A. Hernández Creus,[a] P. Schilardi,[b] S. González,[a] R. C. Salvarezza,[b] and A. J. Arvia*[,b]

[a]*Departamento de Química Física, Universidad de La Laguna, Tenerife, Spain*
[b]*INIFTA, Instituto de Investigaciones Fisicoquímicas Teóricas y Aplicadas, Universidad Nacional de La Plata, La Plata, Argentina*

ABSTRACT

The electrochemical faceting and roughening of polycrystalline Ag and Cu electrodes in aqueous 0.01 *M* $HClO_4$ + 0.5 *M* $NaClO_4$ at 25°C was investigated by applying a symmetric square wave potential reversal technique for 20 h between preset upper and lower potential values in the range 5 Hz < *f* < 5 kHz. The characteristics of treated specimens were followed by voltammetry, Pb underpotential deposition for Ag, and Tl underpotential deposition for Cu, and scanning electron microscopy. For *f* < 50 Hz, the net electrochemical reaction involves the metal electrodissolution in the oxidation half-cycle and metal electrodeposition accompanied by the development of a branched metal topography in the reduction half-cycle. In contrast, for *f* > 50 Hz, the metal electrodissolution/electrodeposition cycling produces local faceting at each metal grain. The amount of soluble species found in the solution after a 20 h potential reversal technique increases as *f* is decreased. Under comparable conditions, both metals behave in a rather similar way, although Cu deposits are always more compact than those resulting from the application of the potential reversal.

Introduction

The electrochemical roughening and faceting of metals based upon the application of different periodic potential routines is an attractive procedure for developing textured metal surfaces.[1-6] This procedure has been extensively employed to modify the surface topography of noble metal electrodes by applying either a periodic potential to these electrodes immersed in an aqueous environment[7] or by electroreducing a hydrous noble metal oxide layer previously built up using an adequate potential routine.[5] Less attention has been paid to the application of these techniques to other lower cost metals of wider practical interest. Previous results on Cu electrodes in aqueous phosphoric acid[8] have shown that either a smooth or a rough topography resulted depending on the frequency of the periodic potential routine. The latter determines the characteristics of the nonstationary diffusion layer built up around the electrode.[8]

This work refers to changes in the topography of polycrystalline Ag and Cu electrodes immersed in an acid electrolyte solution produced by a prolonged application of the potential reversal technique (PRT). Topographic changes are followed by scanning electron microscopy (SEM), and underpotential deposition (upd)/anodic stripping voltammetry of Pb for Ag,[9] and Tl for Cu.[10] For both Ag and Cu, the application of PRT at relatively high frequencies (*f* > 50 Hz) produces electrofaceting at grain domains without a significant increase in surface roughness and only small amounts of soluble metal ionic species in the solution. Under these conditions, a clear long-term smoothing of the metal surface can be noticed. Conversely, at low frequencies (*f* < 50 Hz), branched electrodeposits are formed simultaneously with the appearance of a rather large concentration of metal ions in the solution.

The changes in the electrode topography can be explained as a complex process involving the specific electrochemical kinetics and mechanism of the Ag/Ag^+ and Cu/Cu^{2+} electrode, the participation of ionic transport processes at the solution side, and metal atom surface diffusion.

Experimental

Electrochemical runs were made in a conventional three-electrode Pyrex glass cell using either polycrystalline Ag or Cu working electrodes and Pt counterelectrode plates facing up the working electrode surface. The reference electrode was a saturated calomel electrode (SCE). Working electrodes were subjected to different pretreatments. Thus, Ag electrodes were etched in diluted

* Electrochemical Society Active Member.